

Coexistence of rectilinear and vortex polarizations at twist boundaries in ferroelectric PbTiO_3 from first principles

Takahiro Shimada,^{1,*} Xiaoyuan Wang,¹ Shogo Tomoda,¹ Pavel Marton,² Christian Elsässer,² and Takayuki Kitamura¹

¹*Department of Mechanical Engineering and Science, Kyoto University, Sakyo-ku, Kyoto 606-8501, Japan*

²*Fraunhofer-Institut für Werkstoffmechanik IWM, Wöhlerstraße 11, D-79108 Freiburg, Germany*

(Received 21 October 2010; revised manuscript received 28 January 2011; published 28 March 2011)

Atomic and electronic structures as well as ferroelectricity at $\Sigma 5(001)$ twist boundaries in ferroelectric PbTiO_3 have been investigated using first-principles (*ab initio*) density-functional theory calculations within the local-density approximation. The twist-boundary structure with the coincidence site lattice of O-Pb and O-O is found to be energetically favorable. At the twist boundary, rectilinear spontaneous polarization along the normal direction to the boundary is highly enhanced because of the locally strengthened covalent Pb-O bond, which predominates ferroelectricity in PbTiO_3 . Interestingly, we found vortex or toroidal polarization in the twist-boundary plane coexisting with the rectilinear polarization. The vortex polarization arises from rotational in-plane displacement induced by the twisted misorientation of lattices. An applied tensile strain tends to increase the rectilinear polarization, especially at the twist boundary. On the other hand, the vortex polarization is suppressed upon application of a tensile strain and finally disappears at a critical strain in the TiO_2 layer of the boundary, whereas the PbO layer exhibits the opposite tendency.

DOI: [10.1103/PhysRevB.83.094121](https://doi.org/10.1103/PhysRevB.83.094121)

PACS number(s): 77.80.-e, 61.72.Mm, 68.35.-p, 31.15.A-

I. INTRODUCTION

Ferroelectric perovskite oxides, e.g., PbTiO_3 and BaTiO_3 , are electroceramic materials that exhibit not only ferroelectricity but also a variety of useful electrical properties, including a high dielectric constant as well as piezoelectricity. Because of their multiple functionalities, perovskite oxides have drawn significant attention for technological applications, such as nonvolatile random access memories (FeRAMs), transducers, and electromechanical devices.^{1,2}

Since perovskite oxide ceramics are usually polycrystalline materials, grain boundaries (GBs) are one of the most important planar defects within the material. It is well known that the grain boundaries considerably affect electronic properties. For example, grain boundaries induce nonlinear current-voltage (*I-V*) characteristics and a positive temperature coefficient of resistivity (PTCR).³⁻⁶ It has been reported that these properties are highly dependent on crystallographic misorientation and defect segregation at grain boundaries.⁷⁻⁹ Thus the atomic and electronic structures of grain boundaries in perovskite oxides play a central role in determining the properties, and have been studied both experimentally and theoretically. For instance, tilt grain boundaries in perovskite oxides, including $\Sigma 3(111)$, $\Sigma 3(112)$, $\Sigma 5(210)$, $\Sigma 5(310)$, $\Sigma 13$, $\Sigma 17$, and random grain boundaries, have been actively investigated by means of atomic-resolution transmission electron microscopy (TEM) and scanning TEM (STEM).¹⁰⁻³³ Here, Σ value means the degree of match between the structures of the two grains described by the reciprocal of the ratio of coincidence sites to the total number of sites on the following boundary plane. Some studies have employed *ab initio* (first-principles) density-functional theory (DFT) calculations, and these theoretical calculations have revealed detailed atomic structures, grain-boundary energies, and electronic properties of these materials. On the other hand, the properties of twist boundaries are poorly understood at present because very few investigations have been conducted thus far on tilt grain boundaries. Only limited reports exist so far: Nomura *et al.* studied a $\Sigma 5(001)$

twist boundary in SrTiO_3 by TEM observations, and showed that the twist boundary is atomically sharp and possesses a coincidence site lattice (CSL) structure.³⁴ Astala and Bristowe elucidated on the stability of the CSL structure and electronic properties of the twist boundary.³⁵ However, to the best of the authors' knowledge, ferroelectricity at twist boundaries has never been studied so far in spite of great scientific interest in microstructural properties as well as the technological importance of this aspect for reliability of devices. Only a first-principles study of the interplay between symmetrical tilt grain boundaries and domain walls (DWs) in ferroelectric PbTiO_3 has been reported very recently.³⁶

Since ferroelectricity originates from the delicate balance between short-range covalent interactions and long-range Coulombic interactions,^{37,38} spontaneous polarization is expected to be significantly affected at a twist boundary in which the heterogeneous atomic arrangement should break this balance. For a deeper understanding of ferroelectric properties at twist boundaries, it is essential to elucidate the detailed atomic and electronic structures of these boundaries.

In this study, we investigated ferroelectricity at the $\Sigma 5(001)$ twist boundaries in a typical ferroelectric perovskite, PbTiO_3 , from both atomistic as well as electronic points of view using *ab initio* density-functional theory calculations, which previously have successfully yielded microscopic descriptions of grain boundaries.^{27,32,39,40} Additionally, we have investigated the fundamental effects of strain, which is often strongly coupled with ferroelectricity.⁴¹⁻⁴³

II. COMPUTATIONAL DETAILS

A. Simulation method

Ab initio (first-principles) calculations based on density-functional theory^{44,45} (DFT) were conducted using the Spanish Initiative for Electronic Simulations with Thousands of Atoms (SIESTA) code.⁴⁶⁻⁴⁸ The local-density approximation (LDA) parametrized by Perdew and Zunger⁴⁹ from Ceperley-Alder

data⁵⁰ was used to evaluate the exchange-correlation energy because the LDA function is essential for a correct description of the structural and ferroelectric ground state of PbTiO_3 .^{51,52}

The electron-ion interaction is described by norm-conserving Troullier-Martins pseudopotentials,⁵³ which explicitly include the Pb 5*d*, 6*s*, and 6*p*, the Ti 3*s*, 3*p*, 3*d*, and 4*s*, and the O 2*s* and 2*p* electrons in the valence states. The Pb and Ti pseudopotentials are generated scalar relativistically. The reference configurations and cut-off radii used for pseudopotential generation are listed in Table I.

The electronic wave functions were expanded in a basis set of strictly localized⁵⁴ numerical atomic orbitals (NAOs).⁵⁵ We used a single- ζ (SZ) basis set for the semicore states of Pb and Ti, and a double- ζ plus polarization (DZP) basis set for the valence states of all atoms. Extra shells of 6*d* and 7*s* orbitals were added for Pb. All the parameters concerning the shape and range of the basis functions were determined by a variational optimization method described in Ref. 56.

The reliability of the pseudopotentials and quality of the basis sets were carefully tested for bulk PbTiO_3 shown in Fig. 1(a). The electronic density, Hartree, and exchange-correlation potentials were calculated in a uniform real-space grid⁵⁷ with an equivalent plane-wave cutoff of 200 Ry. A $6 \times 6 \times 6$ Monkhorst-Pack⁵⁸ *k*-point mesh was used to carry out the Brillouin zone (BZ) integrations. The calculated structural parameters, elastic properties, and band-gap energy of tetragonal PbTiO_3 bulk are summarized in Table II. For comparison, the table also includes results of previous DFT calculations using different methodologies, which have already been validated;^{52,63} a plane-wave (PW) basis set with projector-augmented wave (PAW) potentials^{64,65} implemented in the VASP code^{66,67} and a mixed-basis (MB) set⁶⁸⁻⁷¹ with norm-conserving pseudopotentials (NCPP)⁵³ implemented in the MBPP code.⁷² Overall, the structural, elastic, and electronic properties calculated in this study agree well with the previous results using different methodologies. In particular, the tetragonality of lattice *c/a* and the internal atomic coordinates u_z , which are closely related to ferroelectricity, are in very good agreement. These clearly indicate the reliability of the present calculations. It should be noted that the small underestimate in the lattice constants and band-gap energies from the experimental values is not a problem of our pseudopotentials but a well-known issue concerning to the LDA functional and the DFT framework themselves, respectively.

B. Simulation models and procedure

Figures 1(b) and 1(c) show the schematic illustration of the modeling of the $\Sigma 5$ twist-boundary structure and the simulation model of the $\Sigma 5$ (001) twist boundary in ferroelectric PbTiO_3 . The $\Sigma 5$ (001) twist boundary can be constructed by rotating one upper grain by $\tan^{-1}(1/3) = 18.4^\circ$ and the other lower grain by -18.4° around the [001] axis [the misorientation angle is $2\tan^{-1}(1/3) = 36.9^\circ$]. Hence the crystal orientations in the *x* and *y* directions are [210] and $[\bar{1}20]$, respectively, for the upper grain, and $[2\bar{1}0]$ and [120], respectively, for the lower grain. This grain boundary has one

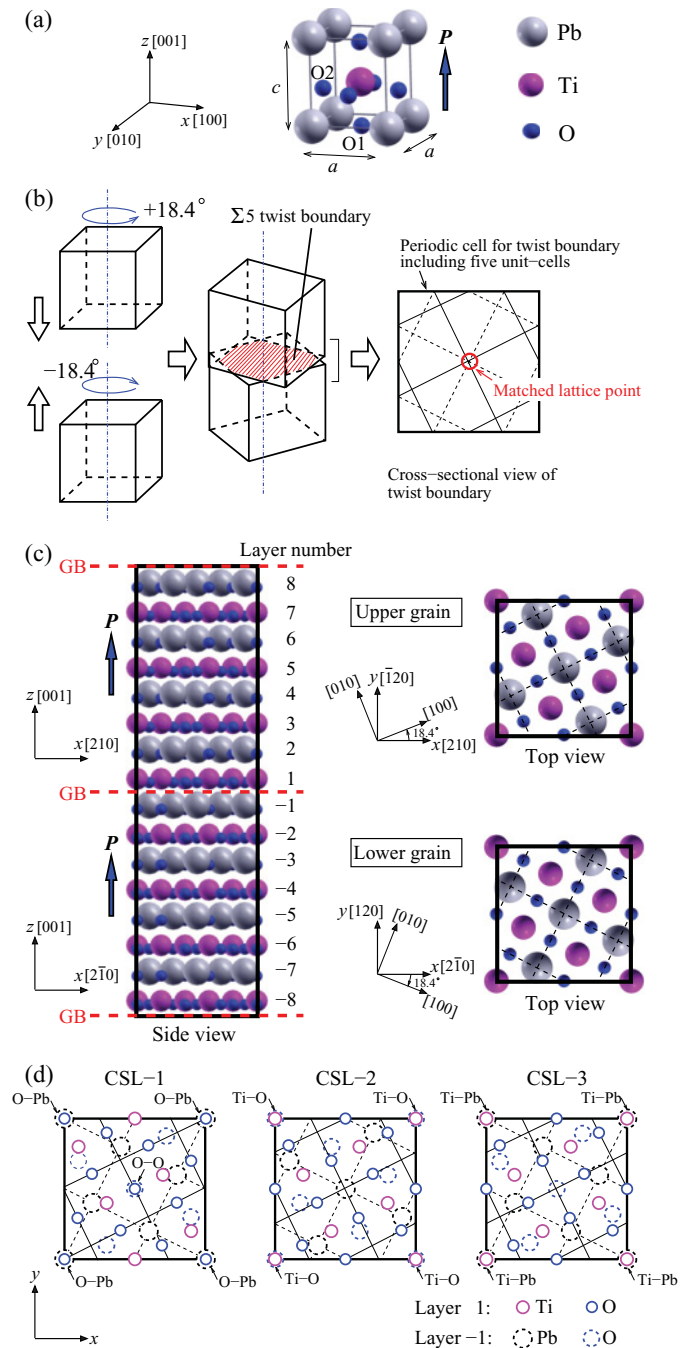


FIG. 1. (Color online) (a) Unit cell of tetragonal PbTiO_3 . (b) Schematic illustration of modeling of $\Sigma 5$ (001) twist boundary in PbTiO_3 . (c) Simulation model of the $\Sigma 5$ (001) twist-boundary structure in ferroelectric PbTiO_3 . The solid box represents the simulation cell. The misorientation angle between the upper and lower grains is $2 \tan^{-1}(1/3) = 36.9^\circ$ around the [001] axis. The position of twist boundaries is indicated by the dashed lines “GB.” The spontaneous polarization \mathbf{P} lies along the [001] direction. (d) Three possible CSL structures at the twist boundary. Only the atoms on layers 1 (TiO_2) and -1 (PbO) across the twist boundary, indicated by the solid and dashed circles, respectively, are shown for clarity. Arrows indicate the CSL site, O-Pb and O-O for CSL-1, Ti-O for CLS-2, and Ti-Pb for CSL-3. The grain-boundary structure shown in (c) is the CSL-2.

TABLE I. Reference configurations and cutoff radii (in bohrs) of norm-conserving Troullier-Martins pseudopotentials for PbTiO₃. The Pb and Ti pseudopotentials are generated scalar relativistically for their ionic configuration (ionic charge of +2), explicitly including their semicore states in the valence.

| Reference configuration | | Pb $6s^2, 6p^0, 5d^{10}, 5f^0$ | Ti $3s^2, 3p^6, 3d^2, 4f^0$ | O $2s^2, 2p^4, 3d^0, 4f^0$ |
|-------------------------|----------|-----------------------------------|--------------------------------|-------------------------------|
| Core radius (bohr) | <i>s</i> | 2.20 | 1.30 | 1.15 |
| | <i>p</i> | 2.60 | 1.30 | 1.15 |
| | <i>d</i> | 2.00 | 1.30 | 1.15 |
| | <i>f</i> | 2.50 | 2.00 | 1.50 |

matched lattice point [see the red circle in Fig. 1(b)] per five square lattices on the (001) boundary plane (see the squares in the same figure), indicating the $\Sigma 5$ grain-boundary structure. Since the three-dimensional periodic boundary condition is applied in the present calculations, the simulation cell contains two equivalent twist boundaries indicated as “GB” at the edge and the center of the cell. The simulation cell consists of 16 (001) atomic layers, altering the PbO and TiO₂ planes along the *z* direction. Thus the total number of atoms in the cell is 200. For descriptive purposes, we assign layer numbers 1 to 8 for the upper grain and -1 to -8 for the lower grain. The spontaneous polarization \mathbf{P} lies along the *z* direction. The initial simulation cell dimensions in the *x*, *y*, and *z* directions are set to $\sqrt{5}a$, $\sqrt{5}a$, and $8c$, respectively, where *a* and *c* are the theoretical lattice constants of the bulk, $a = 3.849\text{\AA}$ and $c = 4.031\text{\AA}$ ($c/a = 1.047$). The Brillouin zone (BZ) integrations were carried out using a $2 \times 2 \times 1$ Monkhorst-Pack⁵⁸ *k*-point mesh. The electronic density, Hartree, and exchange-correlation potentials were calculated in a uniform real-space grid⁵⁷ with an equivalent plane-wave cutoff of 200 Ry.

In this study, we mainly considered a symmetrical coincidence site lattice (CSL) structure for this interfacial alignment of both grains, since it has already been shown both

experimentally and theoretically that the $\Sigma 5$ twist boundary in the perovskite oxides is atomically sharp and possesses the CSL structures.^{34,35} Figure 1(d) shows the three possible CSL twist-boundary structures that were employed in this study. These models have different CSL atomic sites; the O-Pb and O-O sites for the CSL-1 structure, the Ti-O site for CLS-2, and the Ti-Pb site for CSL-3 [see the arrows in Fig. 1(d)]. Additionally, we took into account the structural degrees of freedom of the rigid-body translation of one grain with respect to the other⁴⁰ to confirm that the CSL twist boundary is the stable structure. The rigid-body translation vector \mathbf{t} consists of two components representing the shift in the *x* and *y* directions. For each shift, two grains in the simulation cell are displaced rigidly along the grain-boundary plane with respect to each other. The initial position $\mathbf{t} = (0, 0)$ is set to the CLS-3 structure. The atomic relaxation was conducted using the conjugate-gradient (CG) method until the Hellmann-Feynman forces and the normal stress component of σ_{zz} were less than 5.0×10^{-3} eV/Å and 5.0×10^{-2} GPa, respectively.

For tensile simulations, a small incremental strain $\Delta\epsilon_{zz}$ was applied step by step in the *z* direction to the simulation cell. At each strain, the internal atomic positions were relaxed using the CG method.

TABLE II. Lattice constants, internal atomic coordinates, elastic constants, and band-gap energies E_{gap} of the ferroelectric-tetragonal PbTiO₃ bulk calculated by different computational methodologies. *a* and *c* are the lattice constants of the tetragonal lattice. u_z denotes the internal atomic coordinate in the *z* direction, normalized by the lattice constant *c*. The atoms shown in Fig. 1(a) are included within parentheses. The subscript of the elastic constant c_{ij} follows the Voigt notation. Experimental values are also shown for comparison.

| Methodology code | LCAO + NCPP (This work) | PW + PAW ⁶³ | MB + NCPP ^{52,59} | Experiment ⁶⁰⁻⁶² |
|-----------------------|-------------------------|------------------------|----------------------------|-----------------------------|
| | SIESTA | VASP | MBPP | |
| <i>a</i> (Å) | 3.849 | 3.867 | 3.853 | 3.905 |
| <i>c</i> (Å) | 4.031 | 4.042 | 4.045 | 4.154 |
| <i>c/a</i> | 1.047 | 1.045 | 1.050 | 1.064 |
| u_z [Pb] | 0.000 | 0.000 | 0.000 | 0.000 |
| u_z [Ti] | 0.531 | 0.534 | 0.531 | 0.539 |
| u_z [O1] | 0.083 | 0.090 | 0.092 | 0.114 |
| u_z [O2] | 0.601 | 0.606 | 0.601 | 0.617 |
| c_{11} (GPa) | 289.1 | 284.3 | 293 | 235 |
| c_{12} (GPa) | 122.5 | 114.6 | 129 | 101 |
| c_{13} (GPa) | 99.6 | 91.6 | 99.2 | 98.8 |
| c_{33} (GPa) | 105.9 | 98.7 | 92.5 | 105 |
| c_{44} (GPa) | 67.3 | 61.0 | 67.2 | 69 |
| c_{66} (GPa) | 110.3 | 103.1 | 108.5 | 104 |
| E_{gap} (eV) | 1.63 | 1.65 | 1.62 | 3.5 |

III. RESULTS AND DISCUSSION

A. Grain-boundary energy

The grain-boundary energy γ was evaluated using

$$\gamma = \frac{E_{\text{model}} - E_{\text{bulk}}N}{2S_{\text{GB}}}, \quad (1)$$

where E_{model} , E_{bulk} , N , and S_{GB} denote the total energy of the relaxed simulation model of the twist boundary, the total energy per unit cell of the bulk, the number of unit cells in the simulation model, and the cross-sectional area of the twist boundary, respectively. Figure 2 shows the γ surface of $\Sigma 5$ twist boundary with x and y rigid-body translations. From the structural symmetry, we can find three different local minima on the γ surface, which correspond to three CSL structures shown in Fig. 1(d). This result agrees with the fact that the $\Sigma 5$ twist boundary with the CSL structure was observed experimentally.³⁴ The grain-boundary energies γ of the three CSL twist boundaries are listed in Table III. The twist boundary with the CSL-1 structure is energetically the most favorable because it has the lowest grain-boundary energy. The CSL-1 structure was also found to be the most stable of the SrTiO₃ $\Sigma 5$ twist boundaries.³⁵ The grain-boundary energy of $\gamma = 1.499$ J/m² for PbTiO₃ is close to that of SrTiO₃, $\gamma = 1.2$ J/m².³⁵ In comparison, a smaller grain-boundary energy was reported for a tilt grain boundary in the perovskite oxides: 0.375 J/m² for $\Sigma 3(111)$, 0.686 J/m² for $\Sigma 3(112)$, from 0.948 to 1.114 J/m² for $\Sigma 5(210)$ for different GB-DW arrangements in ferroelectric PbTiO₃,⁷³ 0.52 J/m² for $\Sigma 3(111)[1\bar{1}0]$,^{39,74} 1.02 J/m² for $\Sigma 5(310)[001]$ in SrTiO₃,⁴⁰ and 1.02 J/m² for $\Sigma 5(310)[001]$ in BaTiO₃.⁴⁰

Dasher *et al.* have experimentally shown that the grain-boundary population in the perovskite oxides is correlated to the sum of energies of the surfaces comprising the boundary and grain-boundary energies.⁷⁵ According to this relationship, the grain-boundary population in ferroelectrics can be estimated by calculating a series of surface and grain-boundary energies.

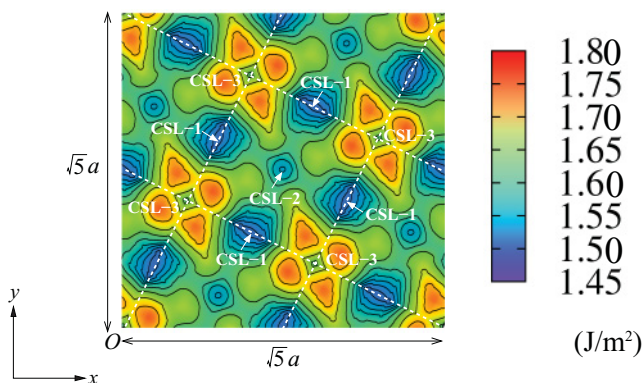


FIG. 2. (Color online) γ surface of the $\Sigma 5$ twist boundary as a function of the rigid-body translations. The white dashed lines indicate the structural periodicity to the rigid-body translations. The origin O is set to the CLS-3 structure.

TABLE III. Calculated grain-boundary energies γ (in J/m²) for three different CSL $\Sigma 5$ twist-boundary structures.

| | CSL-1 | CSL-2 | CSL-3 |
|------------------------------|-------|-------|-------|
| γ (J/m ²) | 1.499 | 1.518 | 1.551 |

B. Atomic and electronic structures at twist boundary

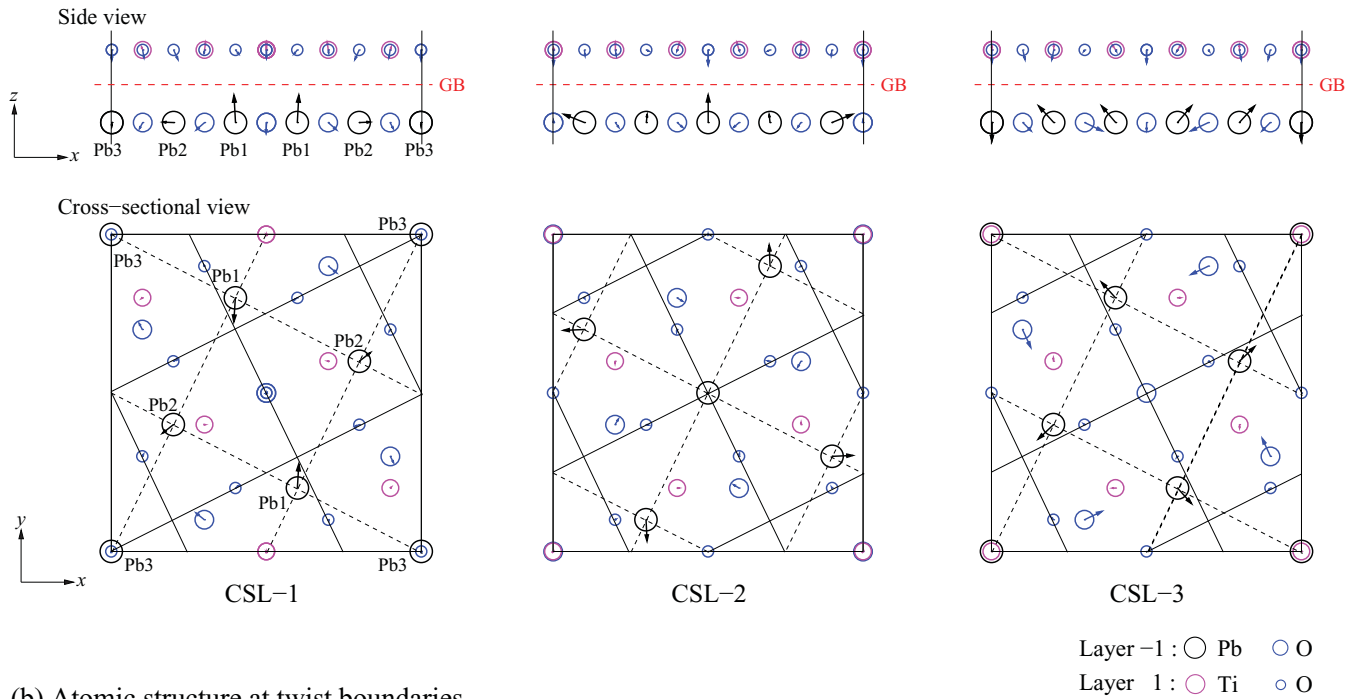
Structural relaxation leads to local volume expansion at the twist boundaries: The interlayer distance between the -1 and 1 layers of 2.452, 2.409, and 2.395 Å in the CSL-1, CSL-2, and CSL-3 structures, respectively, is almost 30% larger than that of 1.874 Å in the bulk. On the other hand, a slight change in the interlayer distance (less than 3%) is found between the adjacent -1 and -2 , and 1 and 2 layers, indicating that volume expansion is highly confined at the twist boundary. Nomura *et al.* experimentally observed such a local volume expansion in a SrTiO₃ $\Sigma 5$ twist boundary using TEM.³⁴ They reported that the twist-boundary structure is atomically sharp and the layer interval at the twist boundary is 1.3 times larger than that of a SrTiO₃ single crystal, which corresponds to our result for PbTiO₃.

Figure 3 shows the atomic displacement and the relaxed atomic structure at the three different CSL twist boundaries. Although each CSL structure shows a different and complicated displacement pattern, some common trends can be discerned: From the cross-sectional views, all in-plane displacement is centrosymmetric. The displacement vector shows that the Pb and Ti atoms separate from each other, whereas the Pb and O atoms and the Ti and O atoms approach each other. Such a displacement pattern should result from repulsive ionic interaction between the cations Pb and Ti, and attractive interaction between the anion O and the cations. In contrast, no in-plane displacement could be observed in a single crystal, wherein the repulsive and attractive interactions are in fine balance because of the regular atomic arrangement.

Another important feature is that the displacement of Pb atoms is much more active than that of the others. Remarkably, some Pb atoms (e.g., Pb1 in the CSL-1 structure) represent a dominant displacement in the z direction of the polar axis (see the side views).

Pb atoms play an important role in determining ferroelectricity in PbTiO₃ because they form a strong covalent Pb-O bond through the hybridization of the Pb $6s$ and O $2p$ orbitals, which leads to large displacement and lattice tetragonality.^{76,77} In fact, the covalent Pb-O bond often characterizes ferroelectric nanostructures, e.g., surfaces,^{41,78} edges in nanowires and surface steps,^{42,43} and an atomically sharp 90° domain-wall structure.⁷⁹ Here, we further investigate the covalent Pb-O bonding character at the twist boundary. Figure 4 shows the distribution of minimum charge density ρ_{min} along Pb-O in the most stable CSL-1 twist-boundary structure. The minimum charge density ρ_{min} is calculated on a line between the Pb and O atoms, which should be one of the parameters representing the covalent Pb-O bond strength.^{42,43} Around the Pb1 atom that shows remarkable displacement, we find the minimum charge density higher than that in the bulk along the corresponding Pb1 and three neighboring O atoms. This suggests that the Pb1 atom forms three strong covalent

(a) Atomic displacement at twist boundaries



(b) Atomic structure at twist boundaries

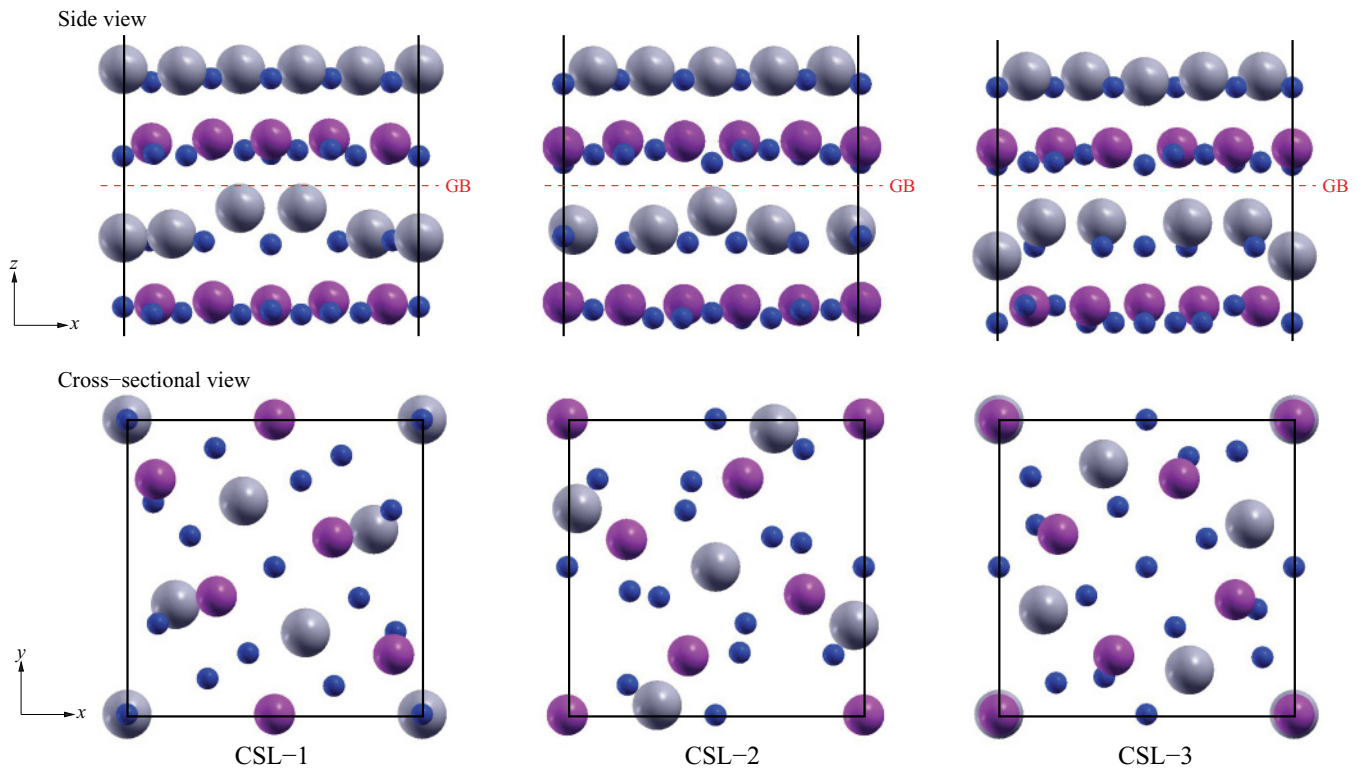


FIG. 3. (Color online) (a) Atomic displacement from the ideal lattice site and (b) relaxed atomic structure at the twist boundaries of the CSL-1, CSL-2, and CSL-3 structures. Only the -1 (PbO) and 1 (TiO₂) layers at the twist boundary are shown for clarity. The Pb atoms with the same number are equivalent because of the centrosymmetry.

bonds with the neighboring O atoms. On the other hand, only a single covalent bond is formed on the Pb2 and Pb3 atoms, in which a small displacement is found [see also Fig. 3(a)]. Thus the dominant displacement of the Pb1 atom is driven by the formation of three strengthened covalent Pb1-O bonds,

while only a single bond on the Pb2 and Pb3 atoms results in their relatively small displacement. It should be noted that a similar bonding character and relationship between the bond strength and displacement can be found in the CSL-2 and CSL-3 structures as well.

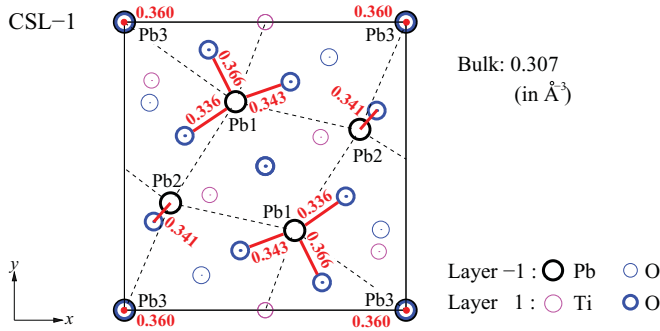


FIG. 4. (Color online) Distribution of minimum charge density ρ_{\min} (in \AA^{-3}) along the Pb-O at the CSL-1 twist boundary across the -1 and 1 layers. Pb atoms with the same number are equivalent because of the centrosymmetry. Only the higher minimum charge density (over 0.200\AA^{-3}) is shown to clear the bonding structure. For reference, the minimum charge density of the covalent Pb-O bond in the bulk is $\rho_{\min}^{\text{bulk}} = 0.307 \text{\AA}^{-3}$.

C. Ferroelectricity at twist boundary in PbTiO_3

To investigate ferroelectricity at the twist boundary, we introduced a ferroelectric distortion of the i th atomic layer,

$$\delta_j^i = \begin{cases} \bar{d}_j(\text{Pb}) - \bar{d}_j(\text{O}) & (\text{PbO layer}), \\ \bar{d}_j(\text{Ti}) - \bar{d}_j(\text{O}) & (\text{TiO}_2 \text{ layer}), \end{cases} \quad (2)$$

where \bar{d}_j denotes the layer-averaged atomic displacement from the ideal lattice site in the j ($= x, y, z$) direction. This definition is often used to discuss polarization distributions in the nanoscale, e.g., at the surfaces^{41,63,78,80} and at the domain walls.^{63,81} Below, we separately discuss the ferroelectricity at the twist boundary (i) in the polar axis of the z direction and (ii) in the in-plane (x and y) directions.

Figure 5 shows the layer-by-layer ferroelectric distortion in the polar axis along the z direction for the three different CSL models. Here, the ferroelectric distortion is normalized by that of the bulk, $\delta_z^* = \delta_z^i / \delta_z^{\text{bulk}}$, where the bulk value δ_z^{bulk} is 0.335 and 0.282\AA for the PbO and TiO_2 layers, respectively. For all the CSL structures, a remarkable increase in δ_z was found at the twist boundary on the layers -1 and 1 : δ_z increased by 35% – 50% with respect to the bulk value on the -1 layer of the PbO plane, while a relatively moderate increase of about 25% was found on layer 1 of the TiO_2 plane. Thus ferroelectricity is enhanced just at the twist boundary, although there is a slight decrease on the adjacent -2 and 2 layers. Considering that remarkable ferroelectricity and large lattice tetragonality in PbTiO_3 arises from a formation of the strong covalent Pb-O

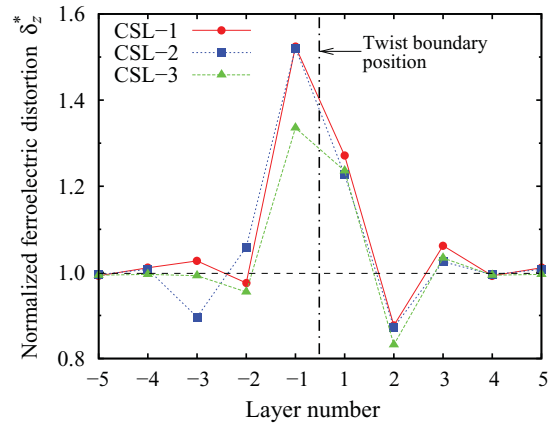


FIG. 5. (Color online) Layer-by-layer ferroelectric distortion normalized by the bulk value $\delta_z^* = \delta_z^i / \delta_z^{\text{bulk}}$ of the three different CSL models. The vertical dotted-dashed line indicates the twist-boundary position; cf. text.

bond,^{76,77} this strong enhancement of ferroelectric distortions must be driven by the partially strengthened Pb-O bond at the twist boundary shown in the previous section. Since the influence of the twist boundary is confined to almost three atomic layers on the upper and lower side grains, the effective thickness of the $\Sigma 5$ twist boundary for ferroelectricity is estimated to be about 13\AA . It is to be noted that, in the middle of the grains, the ferroelectric distortions are almost same as the bulk value, which suggests that the present models should have a sufficient size of the grains to neglect undesirable interactions from neighboring twist boundaries.

Figure 6 shows the vector field of in-plane (in the x and y directions) ferroelectric distortions just at the twist boundary on the -1 (PbO) and 1 (TiO_2) layers for the three different CSL structures. Here, the ferroelectric distortions are calculated via Eq. (2) for each unit plane shown by the dashed squares in Fig. 6. Nontrivial in-plane ferroelectric distortions, the magnitudes of which are almost equal to or more than that of the bulk in the polar direction, were found on the -1 layer of the PbO plane. In addition, the ferroelectric distortion vector represents a vortex or toroidal pattern around the center of the cell O . A similar vortex pattern was also found on layer 1 of the TiO_2 plane. However, the magnitude of the ferroelectric distortion vectors on the TiO_2 plane is much smaller than that on the PbO plane. It should be noted that this in-plane ferroelectric distortion must be induced by the twist-boundary structure because in the PbTiO_3 single

TABLE IV. Radial and azimuthal components of in-plane ferroelectric distortions, δ_r and δ_θ , and toroidal moment τ_z at the twist boundary on the -1 (PbO) and 1 (TiO_2) layers in three different CSL structures. Two values in the CSL-1 structure correspond to sites A and B , respectively [see Fig. 6(a)]. For comparison, ferroelectric distortions in the bulk along the polar axis δ_z^{bulk} are 0.335 and 0.282\AA for the PbO and TiO_2 layers, respectively.

| | Layer number -1 (PbO) | | | Layer number 1 (TiO_2) | | |
|-------|-----------------------------|----------------------------------|-----------------------------|-------------------------------------|----------------------------------|-----------------------------|
| | δ_r (\AA) | δ_θ (\AA) | τ_z (\AA^2) | δ_r (\AA) | δ_θ (\AA) | τ_z (\AA^2) |
| CSL-1 | 0.148, -0.223 | 0.247, 0.265 | 3.939 | 0.050, 0.022 | 0.024, 0.054 | 0.559 |
| CSL-2 | 0.179 | 0.259 | 2.816 | 0.009 | 0.039 | 0.429 |
| CSL-3 | 0.561 | -0.387 | -5.958 | 0.036 | -0.058 | -0.632 |

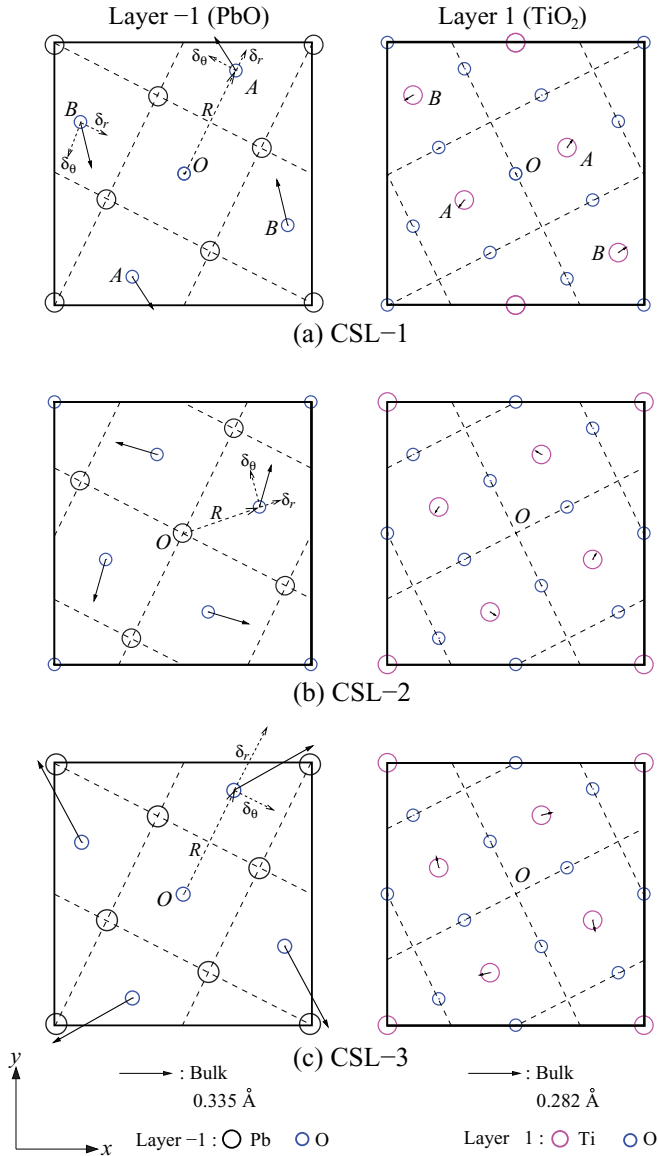


FIG. 6. (Color online) Vector-field representation of in-plane ferroelectric distortions on the -1 (PbO) and 1 (TiO₂) layers at the twist boundary of the (a) CSL-1, (b) CSL-2, and (c) CSL-3 structures. δ_r and δ_θ denote the radial and azimuthal components of the in-plane ferroelectric distortions with respect to the vortex center O , respectively; cf. text.

crystal, there is no ferroelectric distortion in the direction perpendicular to its polar axis. In fact, the in-plane component of δ almost disappears on the adjacent -2 and 2 layers.

To further investigate the vortexlike in-plane polarization state induced at the twist boundary, we first decompose the in-plane ferroelectric distortion to the radial and azimuthal components with respect to the center O , δ_r , and δ_θ , respectively (see also Fig. 6). Then, we introduce a toroidal moment around the z -axis τ_z that represents the vortex polarization state^{82,83} as follows:

$$\tau_z = \sum_k \delta_\theta^k \times R^k, \quad (3)$$

where R^k denotes the position vector of the center of the k th unit plane (see dashed squares in Fig. 6) from the center O . The sum runs over all the unit planes in the simulation cell.

The radial and azimuthal components of the in-plane ferroelectric distortions and the toroidal moment for the three different CSL twist-boundary structures are listed in Table IV. A nonzero and nontrivial toroidal moment was found in all the CSL structures, which clearly signifies the existence of a vortex polarization at the twist boundary. The vortex polarization direction is anticlockwise for the CSL-1 and CSL-2 structures, and is clockwise for the CSL-3 structure, because of the positive and negative τ_z , respectively. A larger toroidal moment is induced on the -1 layer of the PbO plane, while the moment is almost an order of magnitude smaller on layer 1 of the TiO₂. This toroidal moment arises from a rotational in-plane displacement of cations and anions with respect to the center of the cell as discussed in the previous section. In fact, the magnitude of displacement on the PbO and TiO₂ plane corresponds to the toroidal moments.

Such an unusual polarization with vortices is also formed in various ferroelectric nanostructures, for instance, ultrathin films,^{43,84–86} nanowires,⁸² and nanoparticles.^{83,87,88} However, the formation mechanism of vortex polarizations in these nanostructures should be different from the case of the twist boundary: In the ferroelectric nanostructures, the termination

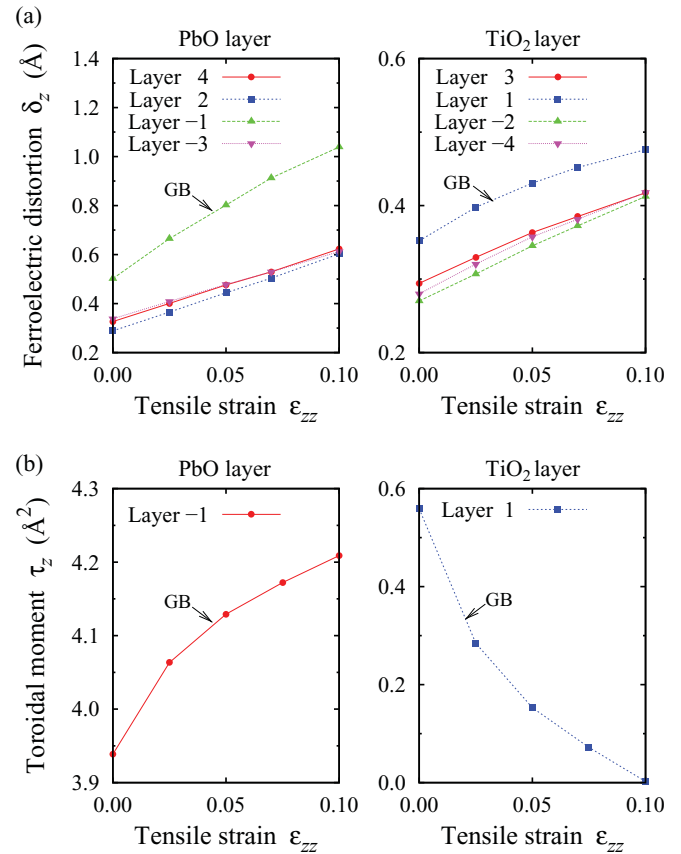


FIG. 7. (Color online) (a) Ferroelectric distortion δ_z and (b) toroidal moment τ_z of the most stable CSL-1 twist-boundary structure as a function of tensile strain ϵ_{zz} . Only the layers near the center twist boundary are shown for symmetry. The -1 and 1 layers at the twist boundary are referred to as “GB.”

of polarization at their surface gives rise to surface charges, which create a depolarizing field that destabilizes the ferroelectric state.^{89,90} To minimize the depolarizing field, the system could adopt a vortex state in which surface charges are compensated for due to the closed polarization loops aligned parallel to the surfaces.^{91,92} The resulting vortex polarization state is thus a natural consequence of energy minimization under geometrical and electrical boundary conditions in the presence of polarization fields. On the other hand, no surface charge appears at the twist boundary because of the absence of free surfaces, however, vortex polarization could be induced by a complex atomic relaxation at the twist boundary. This will be discussed later from the atomistic and electronic points of view.

D. Effect of strain on ferroelectricity at twist boundary

We next briefly report how a tensile strain ε_{zz} applied in the normal direction to the twist boundary affects both rectilinear and vortex polarization. Figure 7 shows the ferroelectric distortion δ_z and toroidal moment τ_z of the most stable CSL-1 twist-boundary model as a function of the tensile strain ε_{zz} . The ferroelectric distortions near the twist boundary increase smoothly with respect to the tensile strain on both the PbO and TiO₂ layers. In particular, δ_z at the twist boundary (layer -1) exhibits a higher increasing rate than the other layers owing to strain concentration at the twist boundary. This indicates that spontaneous polarization at the twist boundary is enhanced by the tensile strain.

The toroidal moment on the PbO layer also increases with increasing strain, whereas that on the TiO₂ layer decreases and finally disappears at a strain of $\varepsilon_{zz} = 0.10$. The same tendency was reported for BaTiO₃ nanowires with vortices wherein the applied axial strain suppressed transverse vortex polarization on the TiO₂ plane of the wires.⁸²

IV. CONCLUSION

In this study, *ab initio* (first-principles) density-functional theory calculations were carried out in order to investigate ferroelectricity at the $\Sigma 5$ (001) twist boundary in PbTiO₃ from atomistic and electronic points of view and the fundamental effects of tensile strain on ferroelectricity at the twist boundary. The coincidence site lattice (CSL) structure of O-Pb and O-O was found to be energetically favorable, and the grain-boundary energy was calculated to be $E_{GB} = 1.499$ J/m². We found the coexistence of both rectilinear spontaneous polarization in the normal direction to the twist boundary and vortex or toroidal in-plane polarization. The rectilinear polarization was highly enhanced at the twist boundary because of the locally strengthened covalent Pb-O bond, which predominates ferroelectricity in PbTiO₃ and characterizes the ferroelectric nanostructures. Vortex polarization at the twist boundary was induced by rotational in-plane displacement resulting from the twisted misorientation of lattices. A tensile strain applied to the twist boundary in the normal direction tends to increase the rectilinear polarization. On the other hand, vortex polarization was suppressed and finally disappeared at a critical strain on the TiO₂ layer of the boundary, while the PbO layer exhibits the opposite tendency.

ACKNOWLEDGMENTS

The authors acknowledge financial support for T.S. and T.K. from the Grant-in-Aid for Scientific Research (S) (Grant No. 21226005) and a Grant-in-Aid for Young Scientists (B) (Grant No. 21760073) from the Japan Society of Promotion of Science (JSPS), for X.W. from the State Scholarship Fund of the China Scholarship Council (CSC), and for P.M. and C.E. from the German Federal Ministry of Education and Research (BMBF Framework Programme WING, Project Code 03X0510).

*shimada@cyber.kues.kyoto-u.ac.jp

¹J. F. Scott, *Ferroelectric Memories* (Springer, Berlin, 2000).

²R. Ramesh, *Thin Film Ferroelectric Materials and Devices* (Kluwer Academic, Boston, 1997).

³M. Fujimoto and W. D. Kingery, *J. Am. Ceram. Soc.* **68**, 169 (1985).

⁴J. Gerblinger and H. Meixner, *J. Appl. Phys.* **67**, 7453 (1990).

⁵M. Kuwabara, K. Morimo, and T. Matsunaga, *J. Am. Ceram. Soc.* **79**, 997 (1996).

⁶K. Hayashi, T. Yamamoto, and T. Sakuma, *J. Am. Ceram. Soc.* **79**, 1669 (1996).

⁷M. Nishi, T. Tanaka, K. Matsunaga, Y. Ikuhara, and T. Yamamoto, *Mater. Trans.* **45**, 2112 (2004).

⁸T. Yamamoto, Y. Sato, T. Tanaka, K. Hayashi, Y. Ikuhara, and T. Sakuma, *J. Mater. Sci.* **40**, 881 (2005).

⁹T. Yamamoto and Y. Ikuhara, *J. Electron Microsc.* **50**, 485 (2001).

¹⁰M. M. McGibbon, N. D. Browning, M. F. Chisholm, A. J. McGibbon, S. J. Pennycook, V. Ravikumar, and V. P. Dravid, *Science* **266**, 102 (1994).

¹¹N. D. Browning and S. J. Pennycook, *J. Phys. D* **29**, 1779 (1996).

¹²N. D. Browning, S. J. Pennycook, M. F. Chisholm, M. M. McGibbon, and A. J. McGibbon, *Interface Sci.* **2**, 397 (1995).

¹³M. M. McGibbon, N. D. Browning, A. J. McGibbon, and S. J. Pennycook, *Philos. Mag. A* **73**, 625 (1996).

¹⁴M. Kim, G. Duscher, N. D. Browning, K. Sohlberg, S. T. Pantelides, and S. J. Pennycook, *Phys. Rev. Lett.* **86**, 4056 (2001).

¹⁵V. P. Dravid, V. Ravikumar, and D. Wolf, *Interface Sci.* **8**, 157 (2000).

¹⁶V. P. Dravid and V. Ravikumar, *Interface Sci.* **8**, 177 (2000).

¹⁷V. Ravikumar and V. P. Dravid, *Ultramicroscopy* **52**, 557 (1993).

¹⁸N. D. Browning, J. P. Buban, H. O. Moltaji, S. J. Pennycook, G. Duscher, K. D. Johnson, R. P. Rodrigues, and V. P. Dravid, *Appl. Phys. Lett.* **74**, 2638 (1999).

¹⁹H. O. Moltaji, J. P. Buban, J. A. Zaborac, and N. D. Browning, *Micron* **31**, 381 (2000).

²⁰Z. Zhang, W. Sigle, F. Phillipp, and M. Rühle, *Science* **302**, 846 (2003).

²¹O. Kienzle and F. Ernst, *J. Am. Ceram. Soc.* **80**, 1639 (1996).

²²N. D. Browning, H. O. Moltaji, and J. P. Buban, *Phys. Rev. B* **58**, 8289 (1998).

²³S.-D. Mo, W. Y. Ching, M. F. Chisholm, and G. Duscher, *Phys. Rev. B* **60**, 2416 (1999).

- ²⁴H. Chang, Y. Choi, J. D. Lee, and H. Yi, *Appl. Phys. Lett.* **81**, 3564 (2002).
- ²⁵C. L. Jia, K. Urban, M. Mertin, S. Hoffmann, and R. Waser, *Philos. Mag. A* **77**, 923 (1998).
- ²⁶C. L. Jia and A. Thust, *Phys. Rev. Lett.* **82**, 5052 (1999).
- ²⁷W. T. Geng, Y. J. Zhao, A. J. Freeman, and B. Delley, *Phys. Rev. B* **63**, 060101(R) (2000).
- ²⁸C. L. Jia, *Philos. Mag. Lett.* **79**, 99 (1999).
- ²⁹C. L. Jia and K. Urban, *Science* **303**, 2001 (2004).
- ³⁰K. J. Dudeck and D. J. H. Cockayne, *Ultramicroscopy* **110**, 1320 (2010).
- ³¹K. J. Dudeck, N. A. Benedek, M. W. Finnis, and D. J. H. Cockayne, *Phys. Rev. B* **81**, 134109 (2010).
- ³²N. A. Benedek, Alvin L. S. Chua, C. Elsässer, A. P. Sutton, and M. W. Finnis, *Phys. Rev. B* **78**, 064110 (2008).
- ³³S. von Althaus *et al.*, *Annu. Rev. Mater. Res.* **40**, 557 (2010).
- ³⁴M. Nomura, N. Ichinose, K. Yamaji, H. Haneda, and J. Tanaka, *J. Electroceram.* **4**:S1, 91 (1999).
- ³⁵R. Astala and P. D. Bristowe, *J. Phys.: Condens. Matter* **14**, 13635 (2002).
- ³⁶P. Marton, T. Shimada, T. Kitamura, and C. Elsässer, *Phys. Rev. B* **83**, 064110 (2011).
- ³⁷R. Resta, M. Posternak, and A. Baldereschi, *Phys. Rev. Lett.* **70**, 1010 (1993).
- ³⁸W. Zhong, R. D. King-Smith, and D. Vanderbilt, *Phys. Rev. Lett.* **72**, 3618 (1994).
- ³⁹S. Hutt, S. Köstlmeier, and C. Elsässer, *J. Phys.: Condens. Matter* **13**, 3949 (2001).
- ⁴⁰M. Imaeda, T. Mizoguchi, Y. Sato, H. S. Lee, S. D. Findlay, N. Shibata, T. Yamamoto, and Y. Ikuhara, *Phys. Rev. B* **78**, 245320 (2008).
- ⁴¹Y. Umeno, T. Shimada, T. Kitamura, and C. Elsässer, *Phys. Rev. B* **74**, 174111 (2006).
- ⁴²T. Shimada, S. Tomoda, and T. Kitamura, *Phys. Rev. B* **79**, 024102 (2009).
- ⁴³T. Shimada, S. Tomoda, and T. Kitamura, *J. Phys.: Condens. Matter* **22**, 355901 (2010).
- ⁴⁴P. Hohenberg and W. Kohn, *Phys. Rev.* **136**, B864 (1964).
- ⁴⁵W. Kohn and L. Sham, *Phys. Rev.* **140**, A1133 (1965).
- ⁴⁶P. Ordejón, E. Artacho, and J. M. Soler, *Phys. Rev. B* **53**, R10441 (1996).
- ⁴⁷D. Sánchez-Portal, E. Artacho, P. Ordejón, and J. M. Soler, *Int. J. Quantum Chem.* **65**, 453 (1997).
- ⁴⁸J. M. Soler, E. Artacho, J. D. Gale, A. García, J. Junquera, P. Ordejón, and D. Sánchez-Portal, *J. Phys.: Condens. Matter* **14**, 2745 (2002).
- ⁴⁹J. P. Perdew and A. Zunger, *Phys. Rev. B* **23**, 5048 (1981).
- ⁵⁰D. M. Ceperley and B. J. Alder, *Phys. Rev. Lett.* **45**, 566 (1980).
- ⁵¹Z. Wu, R. E. Cohen, and D. J. Singh, *Phys. Rev. B* **70**, 104112 (2004).
- ⁵²Y. Umeno, B. Meyer, C. Elsässer, and P. Gumbsch, *Phys. Rev. B* **74**, 060101(R) (2006).
- ⁵³N. Troullier and J. L. Martins, *Phys. Rev. B* **43**, 1993 (1991).
- ⁵⁴O. F. Sankey and D. J. Niklewski, *Phys. Rev. B* **40**, 3979 (1989).
- ⁵⁵E. Artacho, D. Sánchez-Portal, P. Ordejón, A. García, and J. M. Soler, *Phys. Status Solidi B* **215**, 809 (1999).
- ⁵⁶J. Junquera, O. Paz, D. Sánchez-Portal, and E. Artacho, *Phys. Rev. B* **64**, 235111 (2001).
- ⁵⁷J. M. Soler, E. Artacho, J. D. Gale, A. García, J. Junquera, P. Ordejón, and D. Sánchez-Portal, *J. Phys.: Condens. Matter* **14**, 2745 (2002).
- ⁵⁸H. J. Monkhorst and J. D. Pack, *Phys. Rev. B* **13**, 5188 (1976).
- ⁵⁹Y. Umeno and C. Elsässer (unpublished).
- ⁶⁰A. M. Glazer and S. A. Mabud, *Acta Crystallogr.* **34**, 1065 (1978).
- ⁶¹Z. Li, C. M. Foster, and S. K. Chan, *J. Phys. Chem. Solids* **57**, 1433 (1996).
- ⁶²J. Robertson and C. W. Chen, *Appl. Phys. Lett.* **74**, 1168 (1999).
- ⁶³T. Shimada, K. Wakahara, Y. Umeno, and T. Kitamura, *J. Phys.: Condens. Matter* **20**, 325225 (2008).
- ⁶⁴P. E. Blöchl, *Phys. Rev. B* **50**, 17953 (1994).
- ⁶⁵G. Kresse and D. Joubert, *Phys. Rev. B* **59**, 1758 (1999).
- ⁶⁶G. Kresse and J. Hafner, *Phys. Rev. B* **47**, 558 (1993).
- ⁶⁷G. Kresse and J. Furthmüller, *Phys. Rev. B* **54**, 11169 (1996).
- ⁶⁸C. Elsässer, N. Takeuchi, K. M. Ho, C. T. Chan, P. Braun, and M. Fähnle, *J. Phys.: Condens. Matter* **2**, 4371 (1990).
- ⁶⁹K. M. Ho, C. Elsässer, C. T. Chan, and M. Fähnle, *J. Phys.: Condens. Matter* **4**, 5189 (1992).
- ⁷⁰B. Meyer, K. Hummler, C. Elsässer, and M. Fähnle, *J. Phys.: Condens. Matter* **7**, 9201 (1995).
- ⁷¹F. Lechermann, F. Welsch, C. Elsässer, C. Ederer, M. Fähnle, J. M. Sanchez, and B. Meyer, *Phys. Rev. B* **65**, 132104 (2002).
- ⁷²B. Meyer, F. Lechermann, C. Elsässer, and M. Fähnle, Fortran90 Program for Mixed-Basis Pseudopotential Calculations for Crystals (unpublished).
- ⁷³P. Marton and C. Elsässer, *MRS Fall Meeting*, Boston, 2009, p. F9.4.
- ⁷⁴S. Gemming and M. Schreiber, *Chem. Phys.* **309**, 3 (2005).
- ⁷⁵B. E. Dasher, T. Sano, and G. S. Rohrer, *J. Am. Ceram. Soc.* **87**, 670 (2004).
- ⁷⁶R. E. Cohen, *Nature (London)* **358**, 136 (1992).
- ⁷⁷Y. Kuroiwa, S. Aoyagi, A. Sawada, J. Harada, E. Nishibori, M. Takata, and M. Sakata, *Phys. Rev. Lett.* **87**, 217601 (2001).
- ⁷⁸C. Bungaro and K. M. Rabe, *Phys. Rev. B* **71**, 035420 (2005).
- ⁷⁹T. Shimada, Y. Umeno, and T. Kitamura, *Phys. Rev. B* **77**, 094105 (2008).
- ⁸⁰B. Meyer, J. Padilla, and D. Vanderbilt, *Faraday Discuss.* **114**, 395 (1999).
- ⁸¹B. Meyer and D. Vanderbilt, *Phys. Rev. B* **65**, 104111 (2002).
- ⁸²G. Pilania, S. P. Alpay, and R. Ramprasad, *Phys. Rev. B* **80**, 014113 (2009).
- ⁸³I. I. Naumov, L. Bellaiche, and H. Fu, *Nature (London)* **432**, 737 (2004).
- ⁸⁴P. Aguado Puente and J. Junquera, *Phys. Rev. Lett.* **100**, 177601 (2008).
- ⁸⁵T. Shimada, S. Tomoda, and T. Kitamura, *Phys. Rev. B* **81**, 144116 (2010).
- ⁸⁶D. Lee, R. K. Behera, P. Wu, H. Xu, Y. L. Li, S. B. Sinnott, S. R. Phillpot, L. Q. Chen, and V. Gopalan, *Phys. Rev. B* **80**, 060102(R) (2009).
- ⁸⁷I. Münch and E. Huber, *Appl. Phys. Lett.* **95**, 022913 (2009).
- ⁸⁸A. Schilling, D. Byrne, G. Catalan, K. G. Webber, Y. A. Genenko, G. S. Wu, J. F. Scott, and J. M. Gregg, *Nano Lett.* **9**, 3359 (2009).
- ⁸⁹I. P. Batra and B. D. Silverman, *Solid State Commun.* **11**, 291 (1972).
- ⁹⁰R. R. Mehta, B. D. Silverman, and J. T. Jacobs, *J. Appl. Phys.* **44**, 3379 (1973).
- ⁹¹L. Landau and E. Lifshitz, *Phys. Z. Sowjetunion* **8**, 153 (1935).
- ⁹²C. Kittel, *Phys. Rev.* **70**, 965 (1946).